SDMT testing and its use in the numerical modelling of a deep excavation

Alessandra Di Mariano
Centre Internacional de Mètodes Numèrics a l'Enginyeria (CIMNE), Department of Civil and Environmental Engineering, Universitat Politècnica de Catalunya (UPC), Barcelona, Spain, adimariano@cimne.upc.edu

Marcos Arroyo[1], Antonio Gens[2]
Department of Civil and Environmental Engineering, Universitat Politècnica de Catalunya (UPC), Barcelona, Spain, marcos.arroyo@upc.edu[1], antonio.gens@upc.edu[2]

Sara Amoroso
Department of Engineering and Geology, Università di Chieti-Pescara, Pescara, Italy, sara.amoroso@unich.it

Paola Monaco
Department of Civil, Architectural and Environmental Engineering, Università dell'Aquila, L'Aquila, Italy, paola.monaco@univaq.it

ABSTRACT: The role of in situ tests in numerical analyses of deep excavations is investigated. The construction of a metro station in Barcelona required a deep excavation in a densely built urban area. Geological conditions were complex and challenging, involving soft alluvial materials below groundwater level. A comprehensive instrumentation system allowed monitoring the deep excavation-induced movements in the area and finite-element numerical analyses were carried out to reproduce the complex construction process. Results from two different numerical models are compared to field observations. The first model was based on data resulting from conventional analyses of site and laboratory investigations and initial monitoring results. The second model was instead created using only seismic dilatometer data, but using instead a systematic approach to calibrate soil stiffness nonlinearity. Comparison of numerical results and subsequent monitoring show that, although reasonable agreement is obtained for both modelling approaches, the SDMT-based one appears more accurate. Site characterization based on seismic dilatometer data may prove very useful in deep excavation analyses, particularly if the soils are difficult to sample.

Keywords: Deep excavation; nonlinear soil stiffness; DMT/SDMT; field instrumentation; 2D modelling

1. Introduction

The execution of deep excavations in urban environments may represent a risk for existing buildings and structures due their impact on surrounding ground. This risk may be reduced to acceptable limits by a systematic use of accurate models of induced ground movements and monitoring-based validation of such models [1, 2]. Monitoring-based model validation may be, however, difficult to integrate within a streamlined construction progress, particularly if the required model adjustments are important. It is therefore of some interest to introduce early in the process a good estimate of soil behaviour. In situ tests are particularly quick to perform hence the interest in using them as a basis for characterization, with a larger role if undisturbed soil sampling is difficult. Site characterization based only on dilatometer data does give rise to good numerical results [9]. This works shows the benefit of SDMT data in the numerical analysis of deep excavations in soft soils.

The deep excavation described in this paper refers to the construction of Les Moreres station [2], one of the 52 stations of Barcelona L9 Metro Line [3-8] (Fig. 1). It was built with the top-down construction method within permanent diaphragm walls. The ground water table in the area was quite close to the ground surface and geological conditions involved soft deltaic deposits of Holocene age. Minimizing the effects of the excavation on the surrounding structures was crucial to the success of the construction process.

Finite element (FE) numerical analyses were carried out during the design and construction of the station to study the performance of the excavation, which was especially close to a large six-story residential building. A nonlinear constitutive model that captures the soil stiffness dependence on stress-strain levels was selected to characterize the soils at the site. A comprehensive instrumentation system was set in place to monitor excavation-induced movements both in the surrounding ground and in the residential building.

Results from site investigations and laboratory tests were employed for calibration of the initial numerical model, which was later adjusted using monitoring results and then used during construction

Once the construction of the station was completed, the problem was reanalysed emphasizing the role of SDMT [2]. In this study, results from the initial and SDMT based model calibrations are compared to in situ observations.

2. Case study

Les Moreres station [2] is located near the Llobregat River, in a densely built urban area (Fig. 1). One of the buildings near the excavation was selected for settlement assessment before the construction began, being the tallest building within the zone of influence and the closest to it. It is a six-story building, whose plan area is 51 m long and 23 m wide (Fig. 2). Its foundation consists of a reinforced concrete slab with a thickness of 0.7 m. The building is divided into three blocks separated by two full-height expansion joints that extend from roof to ground-floor level. The Northeast edge of the building is at approximately 18 m from the centre-line of the tunnel and at about 9 m from the diaphragm walls of the Station (Fig. 2).

The plan and layout of Les Moreres Station in relation to the six-story building are shown in Figure 2. The station -that has a cross-shaped plan- lacks of a structure above ground and it is about 19 m deep (Fig. 3). The diaphragm wall box is approximately 115 m long, in plan, and has a maximum width of 64 m (Fig. 2). Its construction was previous to the excavation of the L9 tunnel and more than 100 discrete diaphragm panels were used for its construction. Further details on this case study may be found in [2].

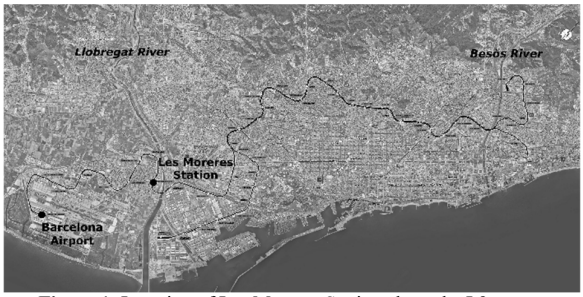

Figure 1. Location of Les Moreres Station along the L9 route.

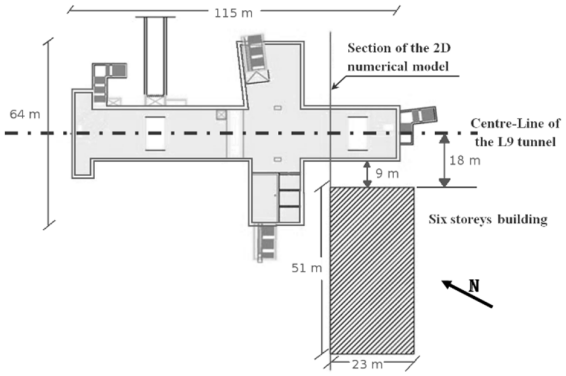

Figure 2. Plan of Les Moreres Station.

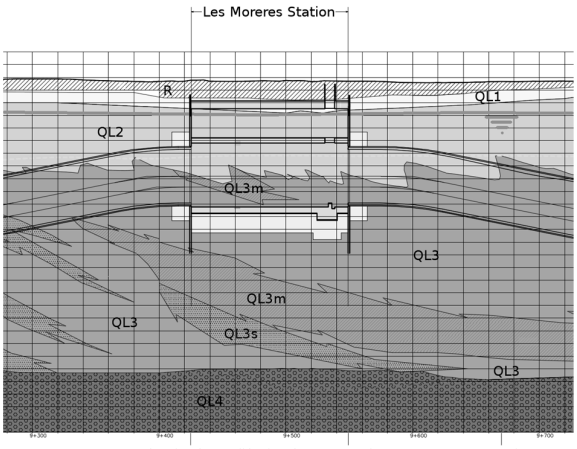

Figure 3. Geological profile in the area of Les Moreres Station.

The geological stratigraphy at Les Moreres Station is as follows (Fig. 3). A superficial fill layer (R) overlies a thin layer of brown fine silts (Ql1), whose combined thickness varies approximately between 1.5 m and 6.0 m. It follows a stratum of grey fine sands, with some gravel intercalations (Ql2), having a width varying from a minimum of nearly 5 m to a maximum of about 9 m. Below, a combination of grey layers of silty clays (with some sandy intercalations) (Ql3), sandy silts (Ql3s) and clays and silts (Ql3m) are encountered, which reach a depth of approximately 42 m. These grey layers are underlain by a stratum of gravels (Ql4) where the confined aquifer is hosted. All of these materials are of Quaternary age. The water table in the area is nearly horizontal (Fig. 3) and it is located at a depth of approximately 3 m from the surface. Pore pressure distribution is close to hydrostatic.

In order to minimize excavation-induced deformations and ground movements, protective measures were incorporated into the design, such as stiff diaphragm wall panels, a low-level jet grouting strut, jet grouting columns as well as specially designed sequences for the excavation and construction of the Station. The low-level jet grouting strut, 3 m in thickness, was installed at a depth of about 18 m, just below the tunnel invert, before the excavation started. Jet-grouted columns behind the vertical joints among the wall panels were executed to reduce ground water inflow into the excavation and accidental piping risk [2].

The six-story building damage risk-assessment and the prediction of the excavation induced ground movements were carried out using numerical methods. FE analyses were executed with the aim of determining the most favourable construction sequence and assess the effectiveness of different solutions for the position and execution of the low-level jet-grouted strut. The damage to the six-story building was predicted to be negligible, according to Burland recommendations [10] and the construction sequence shown in Table 1 was identified as the most favourable one. However, it was deemed necessary to validate the model predictions during construction.

Table 1. Construction activities for the excavation of Les Moreres Station.

	Activity	Start	End
1	Diaphragm walling	15 July 2009	6 Aug 2009
2	Jet-grouted columns behind vertical joints among wall panels	16 Sep 2009	01 Oct 2009
3	Bottom jet-grouted strut	19 Oct 2009	1 Dec 2009
4	EPB tunnel excavation	2 Dec 2009	5 Dec 2009
5	Extra jet-grouted columns behind the diaphragm walls adjacent to the building	9 Dec 2009	23 Dec 2009
6	Tie beams	14 Jan 2010	29 Jan 2010
7	Excavation to main concrete roof slab level (2.5 m depth)	2 Feb 2010	16 Feb 2010
8	Construction of main concrete roof slab	25 Feb 2010	4 Mar 2010
9	Dewatering to 10 m depth	12 Mar 2010	1 Apr 2010
10	Excavation to 2nd concrete slab level (7.5 m depth)	30 Mar 2010	14 Apr 2010
11	Construction of 2nd slab	21 Apr 2010	12 May 2010
12	Dewatering to 18 m depth	3 June 2010	22 June 2010
13	Excavation to deepest level (18.5 m depth)	23 June 2010	27 Oct 2010
14	Construction of bottom concrete slab	25 Aug 2010	8 Nov 2010

3. Initial numerical model

3.1. Overview

Coupled hydro-mechanical numerical analyses were performed with the commercial Code Plaxis2D. The stratigraphy was idealized from the geological profile of the area (Fig. 4). Figure 2 shows the location in plan of the representative section selected for numerical analyses. The section is perpendicular to the L9 longitudinal axis and in its position the length to depth ratio of the excavation is at least 6 while the out-of-plane motion is restricted by the presence of stiff transverse walls [2]. Under these conditions and despite the complex geometric configuration, three dimensional effects do not significantly affect numerical results.

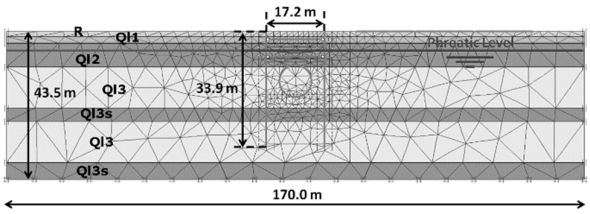

Figure 4. Finite element mesh.

The numerical model reproduced all the activities described in Table 1, except the last one (activity 14). The presence of the jet-grouted columns outside the station wall box (activities 2 and 5, Table 1) was considered in the model by increasing the diaphragm wall stiffness and reducing their interface strength. Low adherence at the interface ground-columns was in fact expected due to soil erosion for jet grout execution and columns retraction at setup [2, 15-16]

3.2. Geometry and discretization

The excavation for the construction of the station in the 2D model is about 17 m wide and 19 m deep, while the total dimensions of the mesh are about 170 m × 44 m (Fig. 4). The position of the mesh lower boundary coincides with the stiff layer of gravels that hosts the deep confined aquifer (QL4 in Fig. 3). The diaphragm walls have a length of about 34 m and the axis of the tunnel is at approximately 15 m below ground level (Fig. 4). The tunnel diameter in the model corresponds to the diameter of the EPB machine used for its excavation (9.4 m).

Fifteen-node triangular elements were used to model the ground layers as well as the low level jet-grouted strut. Figure 4 shows the FE mesh used for the analyses and the simplified soil layering.

The diaphragm walls are considered as simply wished-in-place while for the simulation of the L9 tunnel excavation a volume loss of 0.2% (equal to the in situ observations) was taken into account. This volume loss was simulated in the analysis through the application of the contraction method to the tunnel lining, simulating a reduction of the tunnel cross-section area [17].

The tunnel lining is modelled as a continuous concrete ring, whereas three independent elastic beam elements are used to represent the six-story building made up of three blocks separated by two full-height expansion joints. Five-node Mindlin beam elements [11] represent the diaphragm walls, the station slabs, the tunnel lining and the six-story building adjacent to the Station. In order to take into account the low rotation stiffness of the connection between each station slab and the diaphragm walls, a hinge connection was introduced in the model [2]. Interaction between diaphragm walls or tunnel lining and the surrounding ground is modelled by means of five pairs nodes interface elements.

Horizontal displacements were set equal to zero in the two vertical lateral boundaries, while no displacements were allowed at the lower boundary. The diaphragm walls as well as the tunnel lining were considered fully impermeable. Piezometers measurements were used to define the boundary conditions for the groundwater flow calculations, inside and outside the diaphragm wall box.

Finally, the weight of the building above ground level was taken into account through the application of a uniformly distributed surface load of 60 kPa to the beam elements that represented the building itself.

3.3. Initial calibration

A simple Mohr-Coulomb linear elastic perfectly plastic constitutive model was used to reproduce the behaviour of the fill layer (R) and the jet-grouted low-level strut (Table 2). All the other soil layers were modelled as non-linear elastoplastic materials (Tables 3

and 4) using the so-called Hardening Soil Small model (HSSmall) [12-14]. Variation of soil stiffness at small strains and its non-linear dependency on strain level is considered in the non-linear elastic field, while deviatoric and volumetric hardening is taken into account to model plastic behaviour. On the other hand, elastic and elastoplastic behaviour is assumed for beam and interface elements respectively.

Data from in situ and laboratory investigations were used to determine the mechanical parameters of the soil layers previous to the model calibration (Tables 2, 3 and 4). In situ investigations included boreholes, piezocone tests (CPTu), pressiometer tests and flat dilatometer tests (DMT). Seismic dilatometer tests (SDMT) results were made available late and were not employed in the initial characterization effort.

Laboratory tests comprised oedometer and triaxial tests on boreholes samples beside standard identification tests on both intact and disturbed samples. The combination of compressible grey layers of silty clays (Ql3), sandy silts (Ql3s) and clays and silts (Ql3m) caused great sampling difficulties due to the presence of finely interbedded sandy layers [2, 18].

In Tables 2-4, γ_{sat} and γ_{unsat} represent the soil unit weight below and above the phreatic level, respectively; E_{ref} and c_{ref} the drained Young's modulus of the soil and its cohesion, both relative to a reference stress of 100kPa; ν and ν_{ur} the Poisson's ratio in loading and unloading-reloading stress paths; ϕ the drained friction angle. In the expected stress range, only the materials of the QL2 layer show a slight dilatancy under loading and unloading conditions. A dilantancy angle (ψ) of 2º was assigned to these materials. For the rest of soil layers $\psi = 0$.

The K_0-value for normal consolidated conditions is indicated with K_{0NC}, while m is a power parameter for stress-level dependency of stiffness. The moduli E_{50}^{ref}, E_{oed}^{ref}, E_{ur}^{ref} and G_0^{ref} respectively represent the secant stiffness in standard drained triaxial tests, the tangent stiffness for primary oedometer loading, the unloading/reloading stiffness at engineering strains ($\varepsilon \approx 10^{-3}$ - 10^{-2}) and the reference shear modulus at very small strains ($\varepsilon < 10^{-6}$). All of them are referred to reference stresses of 100kPa. Finally, the symbol $\gamma_{0.7}$ represents the shear strain at which the secant shear modulus G_s^{ref} (relative to a stress of 100 kPa) is decayed to the value of $0.7G_0^{ref}$. Equations (1)-(4) describe the relationship among stiffness parameters.

$$E_{50} = E_{50}^{ref}\left(\frac{c\cdot cot\varphi+\sigma_3'}{c\cdot cot\varphi+p^{ref}}\right)^m \quad (1)$$

$$E_{oed} = E_{oed}^{ref}\left(\frac{c\cdot cot\varphi+\sigma_1'}{c\cdot cot\varphi+p^{ref}}\right)^m \quad (2)$$

$$E_{ur} = 3\cdot E_{50} \quad (3)$$

$$G_0 = G_0^{ref}\left(\frac{c\cdot cot\varphi+\sigma_3'}{c\cdot cot\varphi+p^{ref}}\right)^m \quad (4)$$

Cohesion (c_i), friction angle (ϕ_i) and dilatancy (ψ_i) of interface elements are related to the corresponding properties of the soil materials (c_{soil}, ϕ_{soil} and ψ_{soil}) in contact with the structure, through the R_{inter} parameter (Table 4) as shown in Eqs. (5)-(7).

$$c_i = R_{inter}\cdot c_{soil} \quad (5)$$

$$tan\phi_i = R_{inter}\cdot tan\phi_{soil} \quad (6)$$

$$\psi_i = 0\ if\ R_{inter} < 1.0, if\ not\ \psi_i = \psi_{soil} \quad (7)$$

All soil layers, except the *R* and *QL2* layers, have low permeabilities and are modelled as undrained materials in the numerical analyses, included the jet-grouted low-level strut. On the other side, the *R* and *QL2* layers were modelled as being fully drained.

Table 2. Validated parameters of Mohr-Coulomb linear elastic perfectly plastic materials.

Geomechanical parameter	Fill (*R*)	Jet-grouted low-level strut
γ_{unsat} (kN/m^3)	17.5	19.0
γ_{sat} (kN/m^3)	-	21.5
E_{ref} (MPa)	10	750
ν	0.3	0.3
c_{ref} (kPa)	0.1	400
ϕ (º)	26	27.5
k_x=k_y (m/s)	$4.2\cdot10^{-7}$	$1.3\cdot10^{-10}$
R_{inter}	0.1	1.0

Table 3. Validated parameters of non-linear elastoplastic materials (Part 1)

Geomechanical parameter	QL1	QL2	QL3	QL3s
γ_{unsat} (kN/m^3)	14.7	17.5	13.8	14.7
γ_{sat} (kN/m^3)	19.5	21.3	18.8	19.0
K_{0NC}	0.51	0.47	0.54	0.53
ν_{ur}	0.2	0.2	0.2	0.2
c_{ref} (kPa)	1.0	1.0	1.0	0.2
ϕ (º)	29.0	32.0	27.5	28.0
k_x=k_y (m/s)	$5.7\cdot10^{-7}$	$2.3\cdot10^{-6}$	$1.3\cdot10^{-10}$	$4.3\cdot10^{-10}$

Table 4. Validated parameters of non-linear elastoplastic materials (Part 2)

Geomechanical parameter	QL1	QL2	QL3	QL3s
m	0.9	0.5	0.9	0.7
E_{50}^{ref} (MPa)	19.3	22.5	12.9	14.9
E_{oed}^{ref} (MPa)	17.0	22.5	10.4	14.3
E_{ur}^{ref} (MPa)	57.9	67.5	38.7	44.7
G_0^{ref} (MPa)	72.4	56.3	64.5	74.5
$\gamma_{0.7}$	$1\cdot10^{-4}$	$3.7\cdot10^{-4}$	$3.2\cdot10^{-5}$	$7.4\cdot10^{-5}$
R_{inter}	0.10	0.10	0.15	0.25

3.4. Initial stresses

The initial state of stress in the ground was determined by normally consolidated loading conditions, according to DMT interpretation data. The initial phreatic level was horizontal and located at a depth of 3.5 m from the soil surface. Hydrostatic initial pore pressure distribution was considered.

3.5. Monitoring-based model adjustment

Extensive field monitoring instruments were available for the validation of the numerical model. Figure 5 shows the location of extensometers, inclinometers, precise levelling points on the building, open standpipe as well as vibrating wire piezometers. Data were collected during all construction activities, nevertheless during the execution of the jet grouting columns behind the diaphragm wall panels (activity 5, in Table 1), the only extensometer present in the vicinity of the six-story building, at location B in Fig. 5, broke. This was replaced, just before the first dewatering operations (activity 9 in Table 1) and in situ observations relative to activity 9 were used to validate the numerical model that had to be used for future predictions. This validation stage was deemed particularly necessary as the SDMT data were not available and there was considerable uncertainty about the parameters related to small strain stiffness.

To simulate the excavation process, all solid elements within the diaphragm walls were incrementally removed and the initial hydrostatic pore water pressures were modified appropriately to simulate the first dewatering operations (Figs. 6-7). At this stage of the construction process, the six-story building only suffered small displacements, both in the vertical and horizontal directions (Figs. 8-9). Also, the ground subsurface movements were not important (Figs. 10-11). In all following graphs, negative vertical movements indicate settlements while positive horizontal movements are directed toward the excavation.

Figures 8-11 show for comparison the results from a second numerical analysis carried out after the construction of the station and based just on dilatometer data (see section 5).

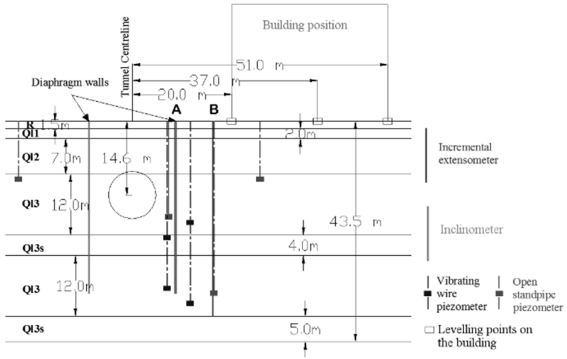

Figure 5. Array of monitoring instruments installed along the section represented by the 2D numerical model.

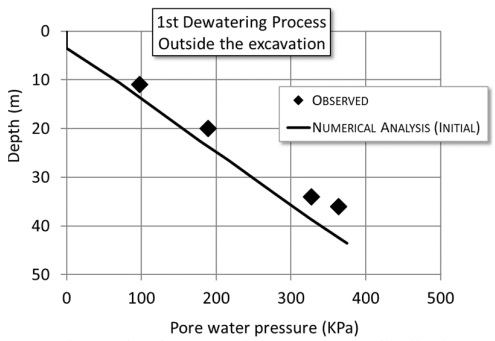

Figure 6. Observed and computed pore pressures distribution outside the excavation on the same side of the building.

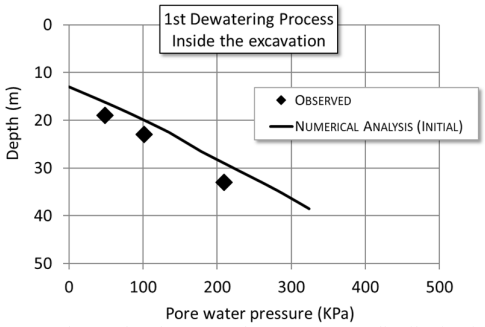

Figure 7. Observed and computed pore pressures distribution inside the excavation.

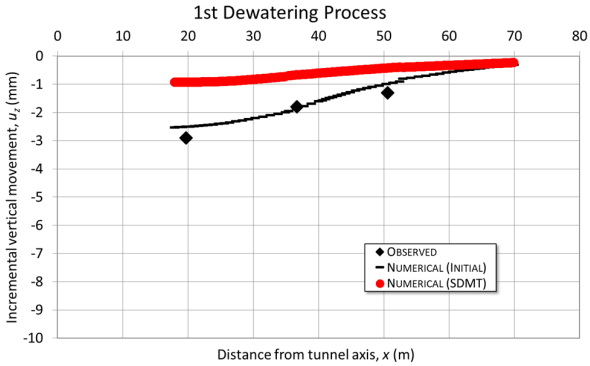

Figure 8. Observed and computed incremental vertical displacement of the six-story building, after the first dewatering process.

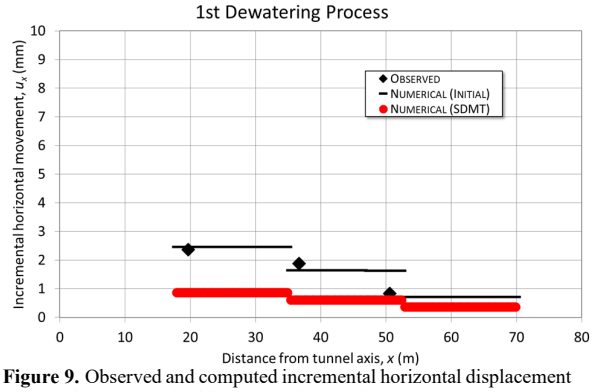

Figure 9. Observed and computed incremental horizontal displacement of the six-story building, after the first dewatering process.

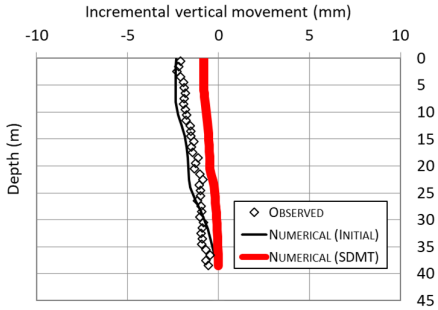

Figure 10. Observed and computed subsurface incremental vertical movement at extensometer location B (Fig. 6), after the first dewatering process.

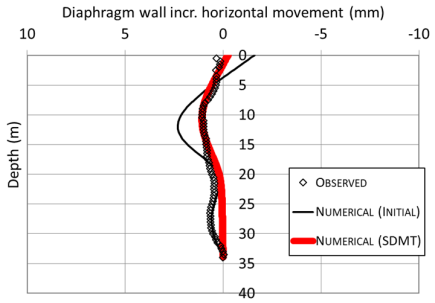

Figure 11. Observed and computed diaphragm wall incremental horizontal movement at inclinometer location A (Fig. 6), after the first dewatering process.

4. SDMT based model

When the construction of the station was completed, a second numerical study was carried out. The numerical model was now calibrated as if only the DMT/SDMT data were available. A new ground model was defined with nine different soil layers identified through dilatometer data [2]. Except for the soil layering, the geometry of the two models does coincide. The constitutive models used in both analyses are the same as well as their initial and boundary conditions. The parameter selection was, however, different. Laboratory data was neglected and profit was taken of recent work systematizing the contribution of SDMT results to soil stiffness decay curve calibration [19, 20].

5. Monitoring results vs model predictions

Once calibrated, the initial model was used to make different types of predictions (Classes A, B and C predictions, using Lambe's terminology) about the ground response associated to the excavation and construction of Les Moreres station [21]. Class C1 predictions (after the event) referred to the first excavation phase (activity 7 in table 1) prior to the first dewatering operations (activity 9, in Table 1). Class B1 predictions (during event) described the excavation to the second slab level (Activity 10 in Table 1). Finally, class A predictions (before event) referred to both the second dewatering phase and the excavation to the deepest level (activities 12 and 13 in Table 1). All the predictions for the SDMT-based are class C1.

All numerical predictions were close to observed surface and subsurface movements, while the residential building final absolute displacements were somewhat overestimated, especially in terms of horizontal movements (Figs. 14-15). Actually, the numerical model did not consider the execution of the bottom slab of the Station which began way before the excavation to the deepest level was completed. Most likely, the real construction sequence, as indicated in Table 1, contributed limiting the ground and building deformations.

Class A initial model predictions were used for a new damage risk-assessment relative to the six-story residential building. Limiting tensile strains as defined by [22] were calculated. Both bending and diagonal tensile strains were considered and, for both modes of deformation, limiting tensile strain values in the range 0-0.05% were found, leaving the building into the category of negligible damage (damage 0) according to Burland recommendations [12]. As a consequence, no further detailed structural evaluation was considered necessary and the construction works continued and ended as planned.

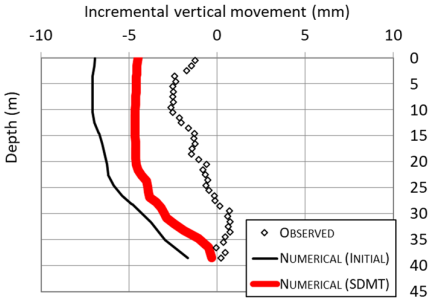

Figure 12. Observed and computed subsurface incremental vertical movement at extensometer location B (Fig. 6), after the excavation to the deepest level.

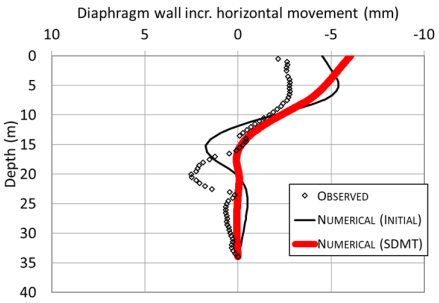

Figure 13. Observed and computed diaphragm wall incremental horizontal movement at inclinometer location A (Fig. 6), after the excavation to the deepest level.

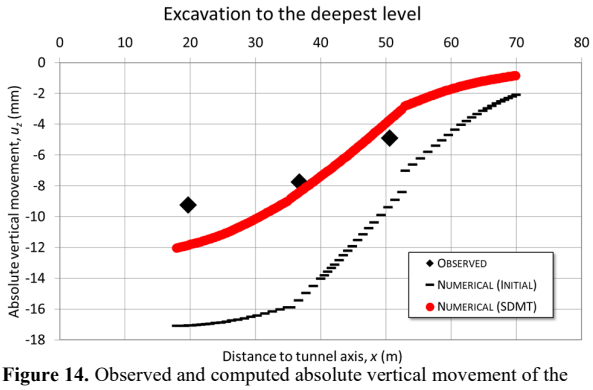

Figure 14. Observed and computed absolute vertical movement of the six-story building, after the excavation to the deepest level.

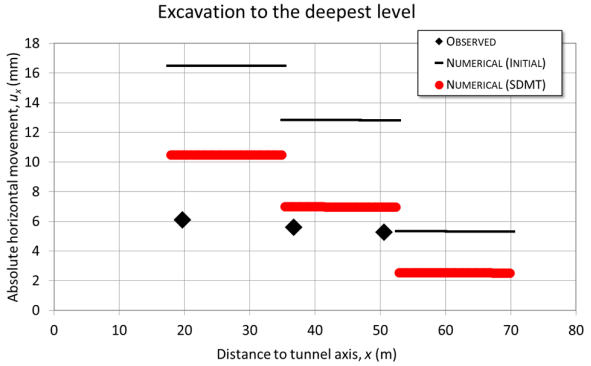

Figure 15. Observed and computed absolute horizontal movement of the six-story building, after the excavation to the deepest level.

In general, numerical results were quite close to observed movements. In the simulation of the first dewatering process, the results from numerical analyses based only on dilatometer data underestimate the building displacements (Figs. 8-9) while reproduce ground subsurface movements with more accuracy (Figs 10-11). Figure 12 shows numerical and observed subsurface incremental ground settlements, relative to the last excavation phase. In this case, the ground settlement distribution obtained with the SDMT-based model is closer to the observations than the distribution obtained from the initial model (Fig. 12).

Incremental ground and diaphragm wall horizontal movements were typically limited, even in the last excavation stage (Figs. 11 and 13). In Fig. 13, numerical results from the initial model are a bit closer to the observed wall movements than the displacements obtained from the SDMT-based model.

Overall, absolute surface and subsurface ground movements were also moderate with maximum observed values smaller than 10 mm (Figs. 14-15). In this case, numerical results from the SDMT-based model are closer to the observations than the movements predicted by the initial model.

6. Discussion

The differences observed between the predictions of the initial model and the SDMT-based model raise the question of what might be the specific parameter changes behind them. Examining the profiles of key parameters versus depth for both models, it appears that the major differences are in the parameters related to small and medium strain response, namely $\gamma_{0.7}$ (Fig. 16) G_0^{ref} (Fig. 17) and E_{ur}^{ref} (Fig. 18). This is not surprising as those are the parameters where the new data and procedures employed in the interpretation of the SDMT-based model were supposed to have a larger impact.

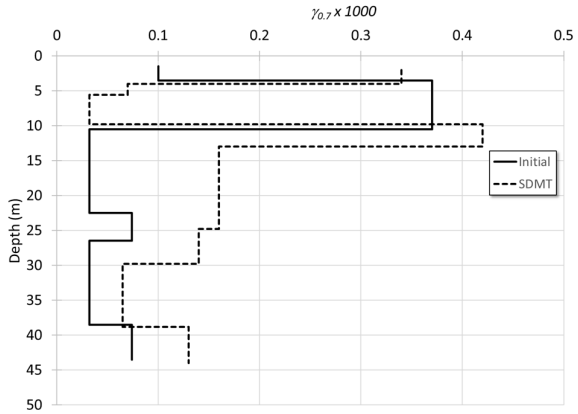

Figure 16. Parameter $\gamma_{0.7}$ vs. depth.

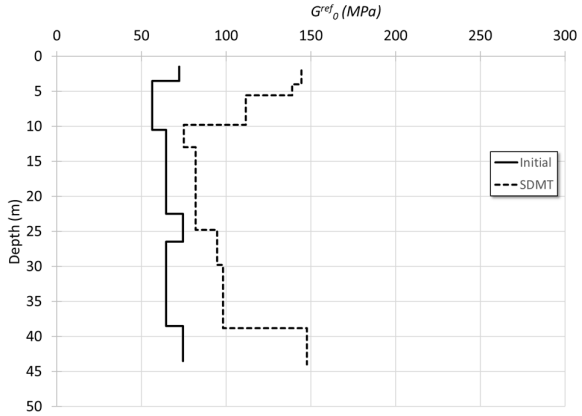

Figure 17. Reference initial shear stiffness moduli vs. depth.

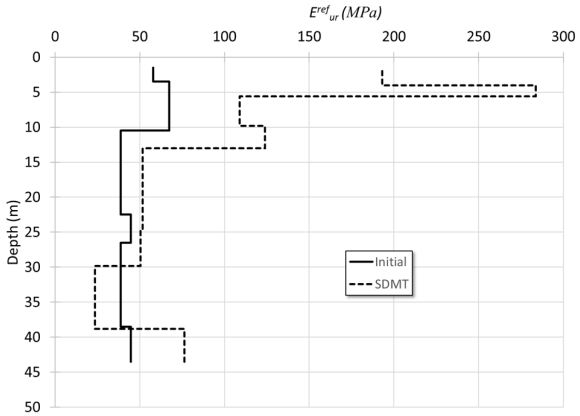

Figure 18. Reference unloading-reloading stiffness moduli vs. depth.

7. Summary and conclusions

The construction of Les Moreres station required a 19 m deep excavation within permanent diaphragm walls, below ground water table, with the use of top-down construction techniques. The geological stratigraphy in the area comprises soft deltaic deposits of Holocene age down to a depth of about 42 m. Initial pore pressure distribution was close to hydrostatic.

The station is located in a densely built urban area where minimization of ground movement was considered a priority during the excavation works. Two-dimensional undrained numerical analyses were run to predict the ground response to the different phases of the construction sequence and the 2D model was properly validated with field monitoring data. A building damage risk assessment was performed for the residential building located near the excavation. Numerical results generally overestimated surface and subsurface final absolute ground movements and building displacements. The excavation and construction process of Les Moreres station was successfully completed and no significant damage was registered in any of the structures adjacent to the station.

After the construction of the station, a second numerical analysis was carried out using only the in situ dilatomer and newly available seismic dilatometer data. Results from this second model showed generally better

agreement with measurements than those of the initial model. The results highlight the value that may be obtained from a characterization based on SDMT tests for problems in which soil stiffness decay plays a major role.

Acknowledgement

The work presented in this article is supported by Infraestructures de la Generalitat de Catalunya, S.A.U.

References

[1] Arroyo, M., A. Di Mariano, A. Gens, E. Alonso, A. García Fontanet, and J. García Germán. "Management of third-party risk in an urban deep excavation project." In Proc., 14th European Conf. on Soil Mechanics and Geotechnical Engineering, 2007, pp. 527–532. Rotterdam, Netherlands: Millpress.

[2] Di Mariano, A, Amoroso, S., Arroyo, M., Monaco P. And Gens A. "SDMT-Based Numerical Analyses of Deep Excavation in Soft Soil", Journal of Geotech. and Geoenviron. Engineering, 145(1), pp. 1-12, 2019. https://doi.org/10.1061/(ASCE)GT.1943-5606.0001993.

[3] Di Mariano, A. & Gens, A. "EPB tunnelling in mixed geological formations: A case study". In: Geotechnical Aspects of Underground Construction in Soft Ground, Taylor & Francis Group, London, 2014, pp. 539-544.

[4] Di Mariano, A., Gesto, J.M., Gens, A. & Schwarz, H. "Ground deformation and mitigating measures associated with the excavation of a new Metro line". Proc. of the 14th ECSMGE, Madrid, 2007, pp. 1901–1906.

[5] Di Mariano A., Persio R., Gens A., Castellanza R. & Arroyo M. "Influence of some EPB Operation Parameters on Ground Movements". EURO:TUN 2009, 2nd Int. Conf. on Computational Methods in Tunnelling, Bochum, 9-11 September, Aedificatio Publishers, 2009, pp. 43-50.

[6] Gens, A., Di Mariano, A., Gesto, J.M. & Schwarz, H. Ground movement control in the construction of a new metro line in Barcelona. In: Geotechnical Aspects of Underground Construction in Soft Ground, Taylor & Francis Group, London, 2006, pp. 389-395.

[7] Gens A., Di Mariano A. & Yubero M.T. "EPB tunneling in deltaic deposits: observations of ground movements". In: Geotechnical Aspects of Underground Construction in Soft Ground, Taylor & Francis Group, 2011, pp. 987-993.

[8] Gens A., Persio R., Di Mariano A., Castellanza R. & Arroyo M. "Relación entre parámetros de una tuneladora EPB y los movimientos del terreno", "Relationship between parameters of an EPB Machine and ground movements". In: 3as Jornadas Hispano-Portuguesas de Geotecnia, Madrid, Cedex, 2009, pp. 433-441. (in Spanish).

[9] Sau, N., Arroyo, M. and Gens A. "Site characterization alternatives for numerical models of a deep excavation", In: Geotechnical and Geophysical Site Characterization 4, Taylor & Francis Group, London, 2013, pp. 1169-1177. ISBN 978-0-415-62136-6.

[10] Burland, J.B. "The assessment of the risk of damage to buildings due to tunnels and excavations". In: Jornada Técnica Aula PaymaCotas, Barcelona 16/12/2008, Movimientos de edificios inducidos por excavaciones: criterios de daño y gestión del riesgo, UPC, 2008, pp. 3-25.

[11] Bathe, K.J. "Finite element analysis in engineering analysis". Prentice-Hall, New Jersey, 1982.

[12] Schanz, T., Vermeer, P.A. & Bonnier, P.G. "The Hardening Soil Model: Formulation and Verification". Beyond 2000 in Computational Geotechnics – 10 years of Plaxis, Balkema, Rotterdam, 1999, pp. 281-296.

[13] Benz, T. "Small-Strain stiffness of soils and its numerical consequences". Ph. D. Thesis, Mitteilungsheft Nr. 55, Institute for Geotechnical Engineering, University of Stuttgart, 2007.

[14] Benz, T., Vermeer, P.A. & Schwab, R. "A small-strain overlay model". Int. Journal for Numerical and Analytical Methods in Geomechanics, 33, pp. 25-44, 2009.

[15] Obrzug, R., and M. Preisig. "Large scale 3D numerical simulations of deep excavations in urban areas—Constitutive aspects and optimization." Mitteilungen der Geotechnik Schweiz 167, pp. 57–68, 2013.

[16] Ho, C. E., C. H. Lim, and C. G. Tan. "Characteristics of bored piles installed through jet grout layer." J. Perform. Constr. Facil. 16 (4), pp. 160–168, 2002. https://doi.org/10.1061/(ASCE)0887-3828(2002)16:4(160).

[17] Plaxis 2D Reference Manual 2018.

[18] Pineda, J. A., M. Arroyo, N. Sau, A. Gens, and N. Pérez. "Testing block samples from silty deposits." In Proc., 4th International Conference on Site Characterization, London, Taylor & Francis, 2012, pp. 1815–1823.

[19] Amoroso, S., B. Lehane, and M. Fahey. "G-γ decay curves in sand by seismic dilatometer (SDMT)." In Proc., 4th Int. Conf. on Geotechnical and Geophysical Site Characterization, 2013, pp. 447–452. London: Taylor & Francis.

[20] Amoroso, S., P. Monaco, B. M. Lehane, and D. Marchetti. "Examination of the potential of the seismic dilatometer (SDMT) to estimate in situ stiffness decay curves in various soil types." Soils Rocks 37 (3), pp. 177–194, 2014.

[21] Lambe, T.W. "Predictions in soil engineering". Géotechnique 23, No. 2, pp. 149-202, 1973.

[22] Burland, J.B., Broms, B.B. & de Mello, V.F.B. "Behaviour of foundations and structures". SOA Report, Session 2, Proc. 9th Int. Conf. SMFE, Tokyo, 2, 1977, pp. 495-546.